Note

Perovskite-type SrTiO₃, CaTiO₃ and BaTiO₃ porous film electrodes for dye-sensitized solar cells

Yuji OKAMOTO and Yoshikazu SUZUKI[*,†]

Graduate School of Pure and Applied Sciences, University of Tsukuba, Ibaraki 305–8573, Japan
*Faculty of Pure and Applied Sciences, University of Tsukuba, Ibaraki 305–8573, Japan

Phase-pure perovskite-type SrTiO₃, CaTiO₃ and BaTiO₃ electrodes have been applied for dye-sensitized solar cells, to obtain higher V_{OC} than TiO₂ electrode. Furthermore, TiO₂/SrTiO₃ and TiO₂/BaTiO₃ composite electrodes have been also prepared. SrTiO₃, CaTiO₃ and BaTiO₃ powders synthesized by solid-state reaction method at 1200°C for 2 h were used to prepare the solar cells. Phase-pure SrTiO₃ and BaTiO₃ cells showed higher V_{OC} than that from TiO₂, but showed lower J_{SC} and efficiency. To utilize the positive effect to increase the V_{OC}, P25 TiO₂/SrTiO₃ and P25 TiO₂/BaTiO₃ composite DSC were prepared. For each series, ~30 wt % addition was favorable to increase the photo-electric conversion efficiency.

1. Introduction

Dye-sensitized solar cells (DSC) have been widely studied because of their high cost merit compared with Si-based solar cells and of their fascinating appearance.[1] DSC with photo-electric conversion efficiency of >10% (or even 12%) have been reported,[2–10] where porous TiO₂ films are generally used as semi-conductor electrodes. Such porous TiO₂ films usually have high specific surface area, and thus, they adsorb plenty of dye molecules, resulting in high current density.[11] To date, our group reported the improvement of efficiency via the nanostructure-control of TiO₂ electrodes.[12–14]

Recently, non-TiO₂ single oxide, such as ZnO,[15] SnO₂,[16] Nb₂O₅[17] and WO₃,[18] have also been extensively studied for DSC electrodes, where these single oxides are used as (A) phase-pure porous electrode, (B) composite electrode with TiO₂, or (C) coating materials for porous TiO₂ network (**Fig. 1**). Besides the non-TiO₂ single oxides, perovskite-type double oxides, e.g., SrTiO₃,[19] CaTiO₃,[20] and BaTiO₃[21] have been applied for the DSC semiconductor electrodes, and they are mainly studied as coating materials for TiO₂ (i.e., type-C in Fig. 1). Some researchers, however, also have reported phase-pure perovskite-type electrodes (type-A). Jayabal et al.[22] reported that SrTiO₃ electrode was effective to obtain relatively higher open-circuit voltage (V_{OC}) of 0.73 eV. SrTiO₃,[22),23] CaTiO₃[24),25] and BaTiO₃[26),27] are n-type semiconductors, and their band-gaps are equal or more than that of TiO₂. Thus, DSC using these perovskite-type semiconductors may exhibit higher V_{OC} than DSC using TiO₂, although the band tuning among electrode, dye and electrolyte is necessary.

In this study, phase-pure SrTiO₃, CaTiO₃ and BaTiO₃ electrodes (type A) have been applied for DSC to obtain higher V_{OC} than TiO₂ electrode. Furthermore, TiO₂/SrTiO₃ and TiO₂/BaTiO₃ composite electrodes (type B) have been also evaluated.

† Corresponding author: Y. Suzuki; E-mail: suzuki@ims.tsukuba.ac.jp
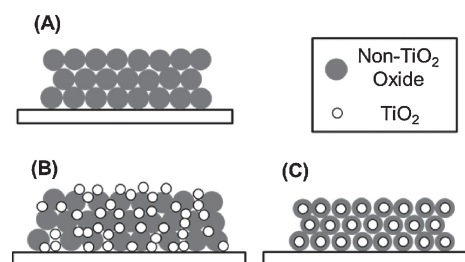
Fig. 1. Non-TiO₂ oxides used for DSC electrodes: (A) phase-pure porous electrode, (B) composite electrode with TiO₂, and (C) coating materials on TiO₂.

2. Experimental

2.1 Preparation of double oxide powders

As for Sr, Ca and Ba sources, commercially available SrCO₃, CaCO₃ and BaCO₃ powders (99.9%, Wako Pure Chemical Industries Ltd., Osaka, Japan) were used, respectively. For Ti source, TiO₂ anatase powder (99%, Kojundo Chemical Laboratory Co. Ltd., Saitama, Japan) was used. Each carbonate powder and TiO₂ powder (1:1 in molar fraction) were mixed by wet-ball milling with nylon balls including steel core for 2 h in ethanol. The slurries were dried by vacuum evaporator for ~30 min, and then the mixture was dried in a 80°C oven for 24 h. The mixed powders were uniaxially pressed at 11.3 MPa to obtain cylindrical pellets. To obtain the double oxides, the pellets were sintered in air at 1200°C for 2 h, with the ramp rate of 5°C/min. After cooling, the pellets were crushed and planetary ball-milled in ethanol at 4 g for 4 h to obtain fine perovskite-type powders. The crystal structure of the powders was determined by X-ray diffractometry (XRD, 40 kV, 40 mA, Multiflex, RIGAKU, Tokyo, Japan).

2.2 Preparation of SrTiO₃, CaTiO₃ and BaTiO₃ photoanodes

The obtained SrTiO₃, CaTiO₃ and BaTiO₃ powders were mixed with polyethylene glycol (molecular weight: 20,000, Wako Pure Chemical Industries Ltd.), 2:1 mass fraction, in an

agate mortar. To prepare the pastes, some distilled water and acetylacetone (dispersant, 99%, Wako Pure Chemical Industries Ltd., Osaka, Japan) were added into the mixed powders. Each mixture was pestled for 20 min.

The $SrTiO_3$, $CaTiO_3$ and $BaTiO_3$ pastes were coated on ITO conducting glass (Type 0052, 10 Ω/sq., Geomatec Co. Ltd., Yokohama, Japan) using the squeegee technique with the electrode area of 1 cm^2. Perovskite-type porous film electrode (type-A) was prepared by sintering at 450°C for 30 min in air. The sintered perovskite electrodes (thickness of ∼10 μm) were immersed in a 0.3 mM ethanol solution of a ruthenium dye (N719, Sigma-Aldrich Co. LLC) at 40°C for 24 h. The microstructure of sintered electrode was observed by scanning electron microscopy (SEM, TM3000 Tablemicroscope, Hitachi, Tokyo, Japan).

2.3 Preparation of TiO_2/perovskite composite photoanodes

To prepare composite photoanodes (type-B), $SrTiO_3$ or $BaTiO_3$ powder described in Section 2.1 was mixed with P25 TiO_2 powder (P25, Nippon Aerosil Co., Ltd., Tokyo, Japan), where the mass fraction of the perovskite powder was 10–50 wt %. TiO_2/ perovskite composite photoanodes were prepared similarly as described above. The film thickness of the composite electrode was set as ∼20 μm, to obtain the homogeneous structure via the thickness direction. As a reference, P25 TiO_2 electrode without the perovskite addition (thickness: ∼20 μm) was also prepared in a similar manner.

2.4 Characterization

The redox electrolyte was composed of 0.5 M LiI (97%, Wako Pure Chemical) and 0.05 M I_2 (99.9%, Wako Pure Chemical) in acetonitrile. Pt-coated ITO was used as a counter electrode. A spacer film with the thickness of 100 μm (T284, Nitoms, Inc., Tokyo, Japan) was used to prepare open-type cells. Solar energy conversion efficiency was measured under simulated solar light, i.e., AM 1.5, 100 mW/cm^2 using a solar simulator (XES-40S1, San-Ei Electric, Osaka, Japan). The light intensity of the illumination source was calibrated by using a standard silicon photodiode (BS520, Bunkoh-Keiki Co. Ltd., Tokyo, Japan). The photocurrent–voltage curves were measured by using a source meter (6241A, ADCMT, Tokyo, Japan).

3. Results and discussion

3.1 Properties of $SrTiO_3$, $CaTiO_3$ and $BaTiO_3$ photoanodes

Figure 2 shows XRD patterns of perovskite-type double oxide powders synthesized at 1200°C for 2 h, which show each constitutent phase was cubic $SrTiO_3$, orthorhombic $CaTiO_3$ and
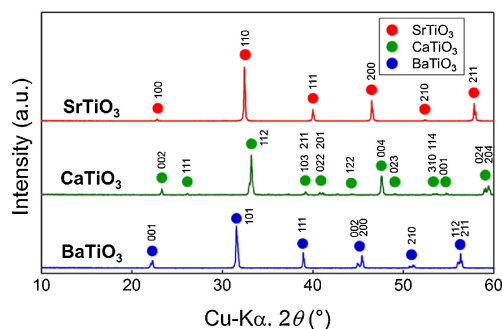
tetragonal $BaTiO_3$, respectively.[28]–[30] Photovoltaic output parameters of DSC with the phase-pure perovskite electrodes (film thickness of ∼10 μm) are summarized in **Table 1**. Values for a widely-used P25 TiO_2 electrode (thickness of ∼20 μm, written in Section 2.3) are also given in the table as a comparison. The cells made from perovskite powders, except the cell made from $CaTiO_3$, showed higher V_{OC} than that from TiO_2. The V_{OC} values depend on the difference between the Fermi level of the oxide and the redox potential of the electrolyte.[31] Since TiO_2 and three perovskite-type double oxides are n-type semiconductors, their Fermi levels are substantially equal to the bottom of the conduction band. As is reported by Jayabal,[22] the conduction band of $SrTiO_3$ is ∼0.2 eV upper than that of TiO_2 anatase. Similarly, as for $CaTiO_3$ and $BaTiO_3$, their schematic band diagams compared with TiO_2 have been given by Jang et al.,[24] and thus, their difference between the Fermi level of the oxide and the redox potential of the electrolyte can be larger than that for TiO_2, which may result in higher V_{OC} as shown in Table 1. Lower V_{OC} for $CaTiO_3$ is then attributable to the mismatch of band structure with dyes; electron transport from the excited dye to $CaTiO_3$ can not be performed efficiently due to its higher conduction band than others.[24] As for the short circuit current density (J_{SC}) and conversion efficiency (η), J_{SC} and η of phase-pure perovskite-type double oxide cells were two-order lower than that of P25 TiO_2. Even taking into account the effect of the thickness, the difference was really remarkable.

To clarify the above reason, appearance and microstructure of these cells are observed, as shown in **Fig. 3** and **Fig. 4**, respectively. Figure 3 indicated that the dye-adsorption for perovskite cells were apparently less than that for TiO_2 cells, which is attributed to the different particle size of the powders (Fig. 4). In this preliminary work, the perovskite powders were prepared by solid-state reaction at 1200°C. Much finer perovskite powders should be necessary to increase the surface area of porous electrodes. **Figure 5** shows the particle-size distributions in perovskite-type cells measured by SEM image analysis. For all samples, particles with the size of ∼0.5 μm were frequently observed. $CaTiO_3$ and $BaTiO_3$ cells contained larger particles than $SrTiO_3$ cell. Since the melting point of $SrTiO_3$ (2080°C) is higher than that of $CaTiO_3$ (1975°C) and that of $BaTiO_3$ (1625°C), grain

Table 1. Photovoltaic output parameters of DSC for phase-pure perovskite electrodes (film thickness of ∼10 μm). Values for a widely used P25 TiO_2 electrode (thickness of ∼20 μm) are also given in the table as a comparison

	TiO_2 (P25)	$SrTiO_3$	$CaTiO_3$	$BaTiO_3$
J_{SC} (mA/cm^2)	13.13	1.28×10^{-1}	1.72×10^{-2}	1.27×10^{-1}
V_{OC} (V)	0.509	0.636	0.488	0.650
FF	0.264	0.464	0.312	0.433
η (%)	1.76	3.78×10^{-2}	2.62×10^{-3}	3.59×10^{-2}

Fig. 2. XRD patterns of perovskite-type double oxide powders synthesized at 1200°C for 2 h.
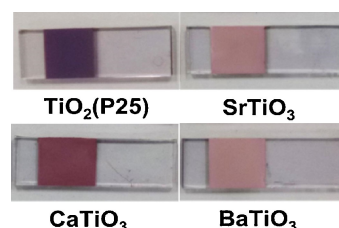
Fig. 3. Appearances of perovskite-type electrodes of DSC (phase-pure porous electrode, type-A).
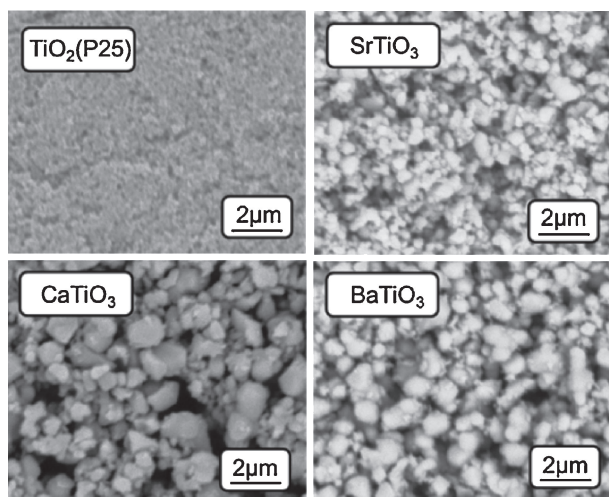
Fig. 4. SEM images of the surface of perovskite-type electrodes of DSC. TiO$_2$ (P25) electrode is also shown as a comparison.
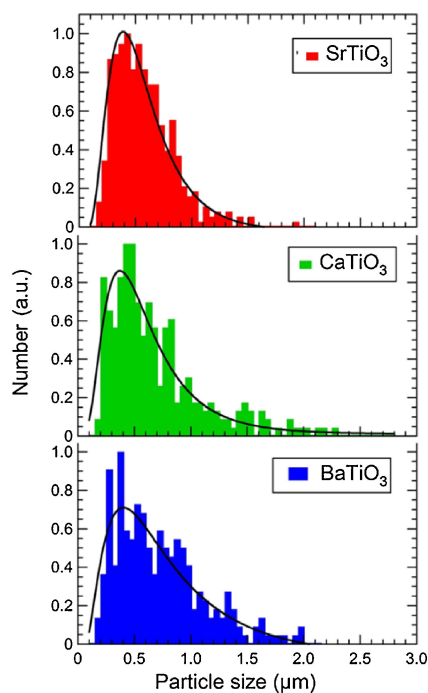
Fig. 5. Particle-size distributions in perovskite-type cells measured by SEM image analysis.

growth of SrTiO$_3$ after solid-state reaction can be smaller than that of CaTiO$_3$ and BaTiO$_3$. Besides some difference in perovskites, larger grain size (compared with P25 TiO$_2$) resulted in less surface contact with TCO and in more possibility of electron–hole recombination at the interface between TCO and electrolyte.[22]

Throughout this section, we can conclude that the submicron-sized perovskite-type powders can be effective to obtain high V_{OC} but cannot be effective to obtain high J_{SC}. Hence, we tried to use the perovskite-type powders not as main phases (type-A) but as second phases in TiO$_2$ matrix (type-B) in the next section.

3.2 Properties of TiO$_2$/perovskite composite photoanodes

In the previous section, SrTiO$_3$ and BaTiO$_3$ showed somewhat higher V_{OC} than TiO$_2$. Hence, these perovskite-type oxides were
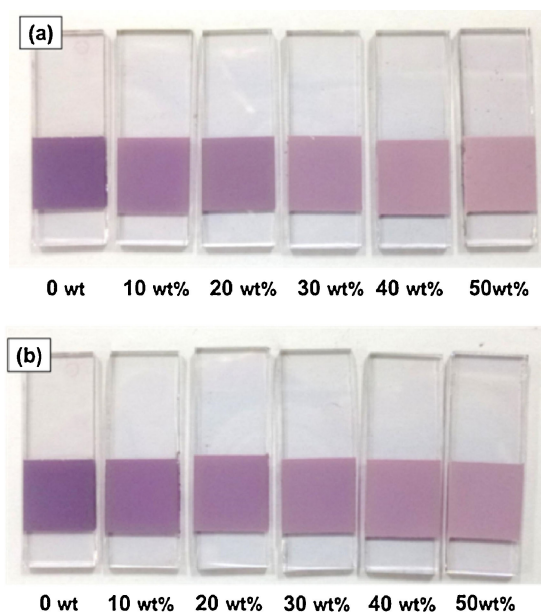
Fig. 6. Apperances of DSC for composite electrodes with TiO$_2$: (a) SrTiO$_3$ (0–50 wt %) + TiO$_2$ and (b) BaTiO$_3$ (0–50 wt %) + TiO$_2$.
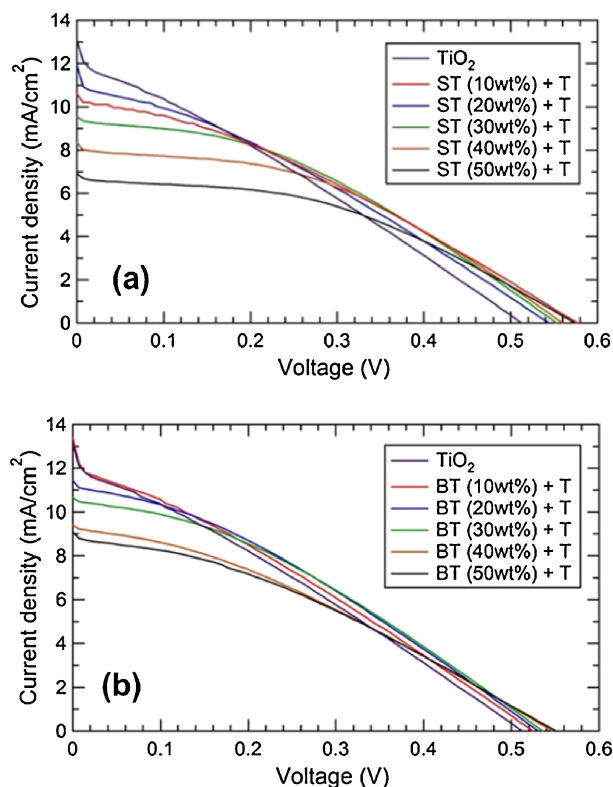
Fig. 7. I–V curves of DSC for composite electrodes with TiO$_2$: (a) SrTiO$_3$ (0–50 wt %) + TiO$_2$, (b) BaTiO$_3$ (0–50 wt %) + TiO$_2$.

then used as second phases. **Figure 6** shows the appearance of P25 TiO$_2$/SrTiO$_3$ and P25 TiO$_2$/BaTiO$_3$ composite electrodes. Dye adsorption seems to decrease with increasing the perovskite powder addition, in good agreement with the previous section. **Figure 7** and **Table 2** show the photovoltaic properties of DSC for composite electrodes with TiO$_2$ (film thickness of ∼20 μm). For both series, with increasing the perovskite-type second phase, V_{OC} increased and J_{SC} decreased. With ∼30 wt % addition of

Table 2. Photovoltaic output parameters of DSC for composite electrodes with TiO_2 (film thickness of $\sim20\,\mu m$). S: $SrTiO_3$, B: $BaTiO_3$

	TiO_2	S (10 wt %) +TiO_2	S (20 wt %) +TiO_2	S (30 wt %) +TiO_2	S (40 wt %) +TiO_2	S (50 wt %) +TiO_2
J_{SC} (mA/cm^2)	13.13	10.61	11.93	9.54	8.33	6.92
V_{OC} (V)	0.509	0.580	0.544	0.559	0.566	0.580
FF	0.264	0.312	0.287	0.368	0.405	0.410
η (%)	1.76	1.92	1.87	1.96	1.96	1.64

	TiO_2	B (10 wt %) +TiO_2	B (20 wt %) +TiO_2	B (30 wt %) +TiO_2	B (40 wt %) +TiO_2	B (50 wt %) +TiO_2
J_{SC} (mA/cm^2)	13.13	13.34	11.45	10.65	9.40	9.09
V_{OC} (V)	0.509	0.530	0.537	0.537	0.551	0.551
FF	0.264	0.260	0.313	0.338	0.321	0.329
η (%)	1.76	1.84	1.93	1.93	1.67	1.65

$SrTiO_3$ or $BaTiO_3$, the composite cells showed higher efficiency than P25 TiO_2. The highest efficiency value was obtained for the composite electrode with 30 wt % $SrTiO_3$, which was 11.4% larger than that of P25 TiO_2.

Although we should also take into account another positive effect by the light-scattering from added large particles, this work suggested a potential use of perovskite-type double oxide for DSC. Aqueous solution process to obtain fine and high-crystallinity perovskite-type double oxide is on going.

4. Conclusions

Phase-pure $SrTiO_3$, $CaTiO_3$ and $BaTiO_3$ electrodes have been synthesized by solid-state reaction methods and applied for DSC to obtain higher V_{OC} than TiO_2 electrode. $SrTiO_3$ and $BaTiO_3$ cells showed higher V_{OC} than that from TiO_2, but lower J_{SC} and efficiency. To utilize the positive effect to increase V_{OC}, P25 TiO_2/$SrTiO_3$ and P25 TiO_2/$BaTiO_3$ composite DSC were prepared. For each series, ~30 wt % addition was favorable to increase the efficiency.

References

1) B. O'Regan and M. Grätzel, *Nature*, **353**, 737–740 (1991).
2) A. Yella, H. W. Lee, H. N. Tsao, C. Y. Yi, A. K. Chandiran, M. K. Nazeeruddin, E. W. G. Diau, C. Y. Yeh, S. M. Zakeeruddin and M. Gratzel, *Science*, **334**, 629–634 (2011).
3) Y. Chiba, A. Islam, Y. Watanabe, R. Komiya, N. Koide and L. Y. Han, *Jpn. J. Appl. Phys.*, **45**, 638–640 (2006).
4) S. Mathew, A. Yella, P. Gao, R. Humphry-Baker, B. F. E. Curchod, N. Ashari-Astani, I. Tavernelli, U. Rothlisberger, M. K. Nazeeruddin and M. Grätzel, *Nat. Chem.*, **6**, 242–247 (2014).
5) P. Wang, S. M. Zakeeruddin, J. E. Moser, R. Humphry-Baker, P. Comte, V. Aranyos, A. Hagfeldt, M. K. Nazeeruddin and M. Grätzel, *Adv. Mater.*, **16**, 1806–1811 (2004).
6) S. Divya, A. Thankappan, C. P. G. Vallabhan, V. P. N. Nampoori, P. Radhakrishnan and A. Mujeeb, *J. Appl. Phys.*, **115**, 064501 (2014).
7) D. Joly, L. Pelleja, S. Narbey, F. Oswald, J. Chiron, J. N. Clifford, E. Palomares and R. Demadrille, *Sci. Rep.*, **4**, 4033 (2014).
8) C. C. Chou, F. C. Hu, H. H. Yeh, H. P. Wu, Y. Chi, J. N. Clifford, E. Palomares, S. H. Liu, P. T. Chou and G. H. Lee, *Angew. Chem., Int. Ed.*, **53**, 178–183 (2014).
9) K. Kurotobi, Y. Toude, K. Kawamoto, Y. Fujimori, S. Ito, P. Chabera, V. Sundstrom and H. Imahori, *Chemistry*, **19**, 17075–17081 (2013).
10) Y. M. Cao, Y. Bai, Q. J. Yu, Y. M. Cheng, S. Liu, D. Shi, F. F. Gao and P. Wang, *J. Phys. Chem. C*, **113**, 6290–6297 (2009).
11) A. Hagfeldt, G. Boschloo, L. C. Sun, L. Kloo and H. Pettersson, *Chem. Rev.*, **110**, 6595–6663 (2010).
12) Y. Suzuki, S. Ngamsinlapasathian, R. Yoshida and S. Yoshikawa, *Cent. Eur. J. Chem.*, **4**, 476–488 (2006).
13) S. Pavasupree, S. Ngamsinlapasathian, Y. Suzuki and S. Yoshikawa, *J. Nanosci. Nanotechnol.*, **6**, 3685–3692 (2006).
14) K. Asagoe, S. Ngamsinlapasathian, Y. Suzuki and S. Yoshikawa, *Cent. Eur. J. Chem.*, **5**, 605–619 (2007).
15) Z. Qifeng, D. S. Christopher, Z. Xiaoyuan and C. Guozhong, *Adv. Mater.*, **21**, 4087–4108 (2009).
16) S. Gubbala, V. Chakrapani, V. Kumar and M. K. Sunkara, *Adv. Funct. Mater.*, **18**, 2411–2418 (2008).
17) K. Sayama, H. Sugihara and H. Arakawa, *Chem. Mater.*, **10**, 3825–3832 (1998).
18) H. D. Zheng, Y. Tachibana and K. Kalantar-zadeh, *Langmuir*, **26**, 19148–19152 (2010).
19) S. J. Wu, X. S. Gao, M. H. Qin, J. M. Liu and S. J. Hu, *Appl. Phys. Lett.*, **99**, 042106 (2011).
20) S. M. Yang, H. Z. Kou, H. J. Wang, K. Cheng and J. C. Wang, *Electrochim. Acta*, **55**, 305–310 (2009).
21) L. Zhang, Y. H. Shi, S. J. Peng, J. Liang, Z. L. Tao and J. Chen, *J. Photochem. Photobiol., A*, **197**, 260–265 (2008).
22) P. Jayabal, V. Sasirekha, J. Mayandi, K. Jeganathan and V. Ramakrishnan, *J. Alloys Compd.*, **586**, 456–461 (2014).
23) S. Yang, H. Kou, J. Wang, H. Xue and H. Han, *J. Phys. Chem. C*, **114**, 4245–4249 (2010).
24) J. S. Jang, P. H. Borse, J. S. Lee, K. T. Lim, O.-S. Jung, E. D. Jeong, J. S. Bae and H. G. Kim, *Bull. Korean Chem. Soc.*, **32**, 95–99 (2011).
25) Q. Fu, J. L. Li, T. He and G. W. Yang, *J. Appl. Phys.*, **113**, 104303 (2013).
26) K. Suzuki and K. Kijima, *Jpn. J. Appl. Phys.*, **44**, 2081–2082 (2005).
27) S. H. Wemple, *Phys. Rev. B*, **2**, 2679–2689 (1970).
28) ICDD-JCPDS No. 86-0178 for cubic $SrTiO_3$.
29) ICDD-JCPDS No. 70-8503 for orthorhombic $CaTiO_3$.
30) ICDD-JCPDS No. 74-4540 for tetragonal $BaTiO_3$.
31) H. Tian and S. Liu, *Adv. Biomed. Eng.*, **8**, 59–63 (2012).